Available online at www.sciencedirect.com

ScienceDirect

Ceramics International 42 (2016) 4562–4566

CERAMICS INTERNATIONAL

www.elsevier.com/locate/ceramint

Structural, magnetic and electrical properties in the pyrochlore oxide $Bi_{2-x}Ca_xIr_2O_{7-\delta}$

Dandan Liang[a,c], Hui Liu[b,*], Ning Liu[a,**], Langsheng Ling[c], Yuyan Han[c], Lei Zhang[c], Changjin Zhang[c]

[a]College of Mechanical and Automotive Engineering, Anhui Polytechnic University, Wuhu 241000, China
[b]Department of Mathematics and Physics, Hefei University, Hefei 230601, China
[c]High Magnetic Field Laboratory, Chinese Academy of Sciences and University of Science and Technology of China, Hefei 230031, China

Received 20 November 2015; received in revised form 25 November 2015; accepted 26 November 2015
Available online 2 December 2015

Abstract

$Bi_{2-x}Ca_xIr_2O_{7-\delta}$ ($x=0$, 0.1, 0.2, 0.3, and 0.4) pyrochlore iridates were prepared by the solid-state reaction method in air. In this paper we reported a systematic study of hole-doped $Bi_{2-x}Ca_xIr_2O_{7-\delta}$ by performing crystal structure, electrical transport and magnetic measurements. A high-crystallized $Bi_{2-x}Ca_xIr_2O_{7-\delta}$ with a cubic structure was obtained. Because Bi^{3+} was substituted in a random way by Ca^{2+} which has relatively smaller ionic radius, disorder and phononic oscillations were induced and the the length of Ir–O bands were reduced. The doped samples were found to exhibit metal–insulator transition. Magnetic measurements on the doping samples indicated a shift towards nonmagnetic Ir^{5+}, and the anti-ferromagnetism was weakened.

Keywords: C. Magnetic properties; D. Transition metal oxides; Metal–insulator transition

1. Introduction

The pyrochlore iridates, $A_2Ir_2O_7$ (A=Y, Bi or lanthanide elements) have attracted much attention on account of spin-orbit coupling (SOC) and correlations for Ir, and provide an ideal setup to study the interplay of correlations, frustration and band topology [1–5]. Various novel phases have been predicted to potentially exist in these compounds and may be accessed by tuning the A-site elements, for instance fractionalized topological insulators [1,6,7], quantum spin liquids [8], topological semimetal with Fermi arcs [1], Weyl semimetal states [1,9], axion insulator [10,11] with bulk magnetic order and large magnetoelectric effect. Substantially experimental efforts have been made to explore their magnetic properties and their electronic structures which are strongly coupled with the magnetic ground states [1,12]. Experimentally, most of the compounds exhibit metal–insulator transition (MIT) in accordance with magnetic phase transitions. Systematic replacement of A-site ions [13,14] indicated that the temperature of the metal–insulator transition, T_{MIT}, decreases with increasing the ionic radius of A (from Y to Pr), and the series goes from magnetic insulators to unconventional metallic systems without magnetic ordering.

$Bi_2Ir_2O_7$ offers an opportunity to distinguish the interesting properties due to the iridium ions and the rare-earth with magnetic moment or f electrons. The muon spin relaxation study [15] showed that $Bi_2Ir_2O_7$ remains metallic down to sub-Kelvin temperatures and provided evidences for a continuous transition into a long-range magnetically ordered state at approximate 2 K. The low temperature state is likely to be a weakly ferromagnetic metal with small magnetic moment. $Bi_2Ir_2O_7$ sits between the Eu and Nd pyrochlore iridates in terms of its lattice constant. But Bi^{3+} ion has a larger ionic

*Corresponding author. Tel.: +86 55162158260.
**Corresponding author. Tel.: +86 13 905531609.
E-mail addresses: liuhui@hfuu.edu.cn (H. Liu), liuning.szsz@163.com (N. Liu).

http://dx.doi.org/10.1016/j.ceramint.2015.11.149
0272-8842/

radius than any of the other reported pyrochlore iridates. This substance shows many features in common with $Pr_2Ir_2O_7$ [16,17], which has a larger A-site ionic radius. The reduced magnetic moment of the iridium ions and the reduced ordering temperature for this compound are likely due to the larger ionic radius of Bi. Although there are some advances, the precise nature of the magnetic and transport properties in this compound is still not completely understood.

In the present work, we have performed x-ray diffraction, Raman scattering, electric transport, magnetic and specific heat measurements on the polycrystalline $Bi_{2-x}Ca_xIr_2O_{7-\delta}$. With the increase of Ca content, the lattice constant decreased continuously, and these substitutions were accompanied with important changes in the local geometry around Ir. We observed an obvious metal–insulator transition in all doped compounds. The magnetic measurements examined the contributions of Ca^{2+} doping to the frustrated magnetism at different temperature. The results showed a weakening of antiferromagnetism (AFM) in all samples.

2. Experiment

Polycrystalline samples of $Bi_{2-x}Ca_xIr_2O_{7-\delta}$ ($x=0$, 0.1, 0.2, 0.3 and 0.4) were synthesized by the solid-state reaction method. The starting materials, powder of Bi_2O_3 (purity 99.99%), IrO_2 (99.95%) and $CaCO_3$ (99.99%) were mixed thoroughly according to the stoichiometric ratio with 5 wt% excess IrO_2. The mixed powder samples were pressed into flake and heated in air at temperatures between 900 °C and 950 °C for about 8 days with several intermediate grindings.

The chemical compositions and distribution were carefully determined by the energy dispersive x-ray (EDX) spectrometry. The EDX spectra for $Bi_{2-x}Ca_xIr_2O_{7-\delta}$ demonstrated that the actual composition of Ca^{2+} was a little more than the named, but increased with the change of doping composition, x. The structure and phase purity were checked by the Rigaku-TTR3 x-ray diffractometer using high-intensity graphite monochromatized Cu Ka radiation. The Raman scattering measurements were performed using a Horiba Jobin Yvon T64000 Micro-Raman instrument with a Kr^+–Ar^+ mixed gas laser ($k=514.5$ nm) as an excitation source in a backscattering geometry. The variation temperature was realized by using a closed He-gas cycle refrigerator established on the machine. The resistivity measurement was carried out by the conventional four-probe method from 3 K to 300 K. The DC magnetization was measured by a Magnetic Property Measurement System (Quantum Design MPMS 7 T-XL) with a superconductive quantum interference device (SQUID). Specific heat measurements were performed by a thermal relaxation method (Quantum Design PPMS).

3. Results and discussion

Fig. 1 gives the powder XRD patterns at 300 K for $Bi_{2-x}Ca_xIr_2O_{7-\delta}$ ($x=0$, 0.1, 0.2, 0.3 and 0.4). It shows that the structures of all the Ca-doped samples keep cubic cell belonging to the space group Fd-3m. As illustrated by the dashed line, XRD peaks of compounds shift slightly to higher 2θ positions. The lattice constant a (refining the XRD patters by the Rietveld method using the Rietica program) versus the Ca-content x was plotted inside Fig. 1. The exact values were shown in Table 1. The lattice parameter of parent material ($x=0$) is consistent with that of the previous report [18]. The lattice parameters of the samples of $x=0.1$–0.4 obey the Vegard's law, which suggests that the Ca substitutions for the Bi site have been achieved in $Bi_{2-x}Ca_xIr_2O_{7-\delta}$. The lattice constant a decreases with the increase of the doping content in $Bi_{2-x}Ca_xIr_2O_{7-\delta}$, which is due to the smaller ionic radius of Ca^{2+} ($Ca^{2+}=1.12$ Å, $Bi^{3+}=1.17$ Å).

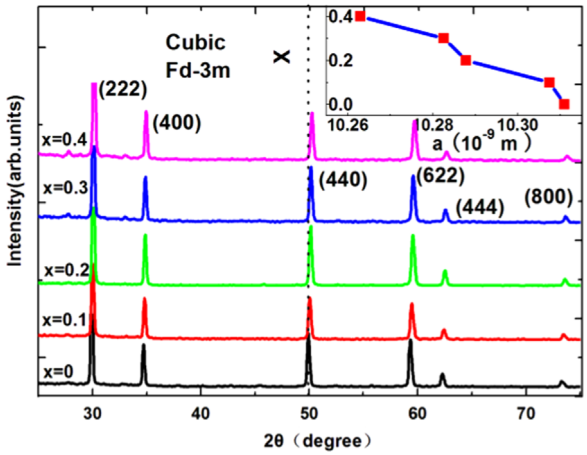

Fig. 1. (Color online) (a) powder x-ray diffraction (XRD) patterns at 300 K for $Bi_{2-x}Ca_xIr_2O_{7-\delta}$ ($x=0$, 0.1, 0.2, 0.3 and 0.4); the inset in figure shows the lattice constants a.

Table 1
Estimated different parameters of $Bi_{2-x}Ca_xIr_2O_7$.

Composition x	The real Ca content	a (10^{-10} m)	T_{MIT} (K)	θcw (K)	C (emu K/Oe mol f.u)
0.0	–	10.312	–	−45.8	0.035
0.1	0.132	10.308	14.106	−17.5	0.015
0.2	0.239	10.288	18.841	−2.7	0.013
0.3	0.341	10.283	28.744	14.5	0.011
0.4	0.463	10.263	39.204	13.2	0.015

Raman spectra for all the $Bi_{2-x}Ca_xIr_2O_{7-\delta}$ samples were measured at 300 K, as shown in Fig. 2(a). For the pyrochlore iridates whose space group is Fd-3m, the irreducible representations of Raman active phonons are $A_{1g}+E_g+4F_{2g}$ [19,20]. The spectrum of $Bi_2Ir_2O_7$ exhibits five conspicuous peaks at the wave numbers of 295.6 cm^{-1}, 391.8 cm^{-1}, 477.8 cm^{-1}, 557.6 cm^{-1} and 663.3 cm^{-1}, respectively. The front four peaks are corresponding to the active Raman modes, which are named as F^2_{2g}, E_g, F^3_{2g} and A_{1g} modes respectively. The peak at 663.3 cm^{-1}, labeled as T_1 do not agree with the ratio of any irreducible, has been reported as second order scattering for pyrochlore oxides [20–22]. In the pyrochlores $A_2Ir_2O_6O'$, O′ ion occupies the 48f site (ζ, 1/8, 1/8), the coordinate value of ζ is mainly determined by the radius of A

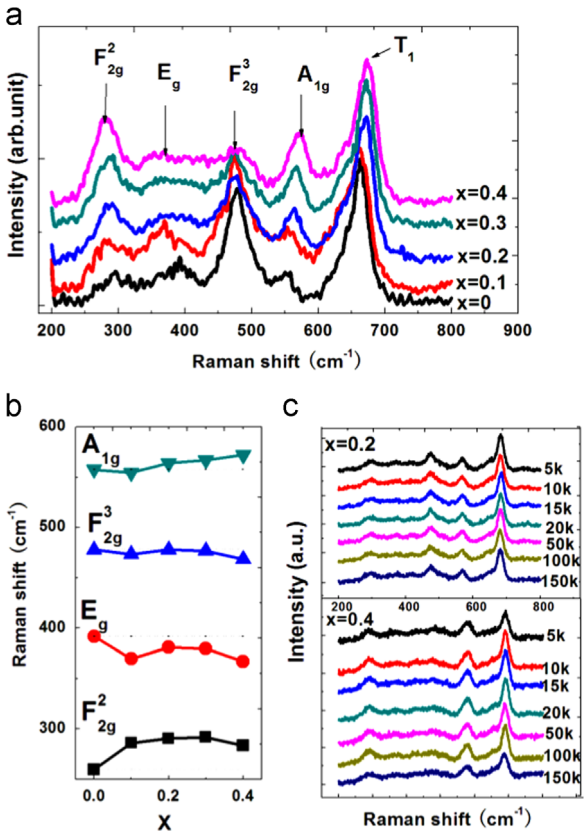

Fig. 2. (a) Raman spectra at 300 K for $Bi_{2-x}Ca_xIr_2O_{7-\delta}$ (x=0.0, 0.1, 0.2, 0.3 and 0.4); (b) the active Raman modes as a function of x with the dotted horizontal lines for reference; (c) the temperature dependence of the spectra for $Bi_{1.8}Ca_{0.2}Ir_2O_{7-\delta}$ and $Bi_{1.6}Ca_{0.4}Ir_2O_{7-\delta}$.

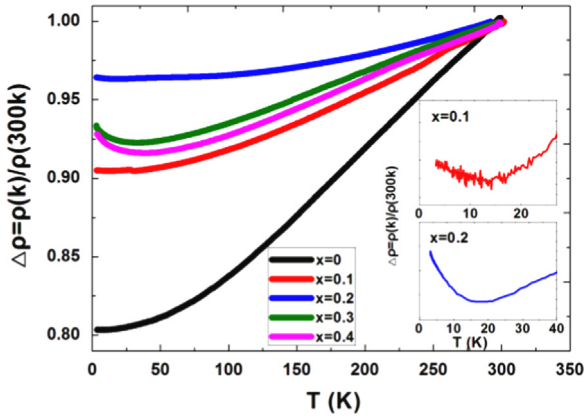

Fig. 3. Electrical resistivities normalized by $\Delta\rho=\rho(k)/\rho(300k)$ as a function of temperature of $Bi_{2-x}Ca_xIr_2O_{7-\delta}$ for x=0, 0.1, 0.2, 0.3 and 0.4. The enlarged view of electrical resistivity for x=0.1 and 0.2 samples.

site [1,12]. The middle-frequency modes (E_g, F^3_{2g}) are mainly contributed by the Ir–O bands, and the F^2_{2g}, A_{1g} modes are mainly associated with the A–O′ bands. With the increase of x, the Raman shifts of E_g and F^3_{2g} modes decrease, but the F^2_{2g} and A_{1g} modes shift significantly to higher frequencies, as shown in Fig. 2(b). These trends are due to the hybridization among Bi (6s), O (2p) and Ir (5d) orbitals, accounting for the increasing of the Ir–O chemical bands length and the shortening of A–O′ bands [21,23]. Fig. 2(c) shows the temperature dependence of the spectra for x=0.2 and 0.4. Neither of the peaks shifts when the temperature incrementally changes from 5 to 150 K, which implies that the temperature affects the motions in this compound slightly.

Fig. 3 shows the temperature dependence of the electrical resistivity which is normalized by

$$\nabla\rho=\rho\_((T))/\rho\_((300\ \mathrm{k})) \quad (1)$$

The parent sample $Bi_2Ir_2O_7$ (x=0) shows metallic state, and the Ca-doped samples (x=0.1–0.4) exhibit metal–insulator transition at 14.106, 18.841, 28.744 and 39.204 K, respectively. The temperature of metal–insulator transition (T_{MIT}) increases monotonically as the ionic radius of Bi site decreases. For the data just below T_{MIT}, we estimated the energy gap by assuming the equation:

$$\rho\_((T))=\rho\_((0))\exp(E/T) \quad (2)$$

E is the energy gap. The estimated E for the doped samples is 15, 38, 36 and 408 K, respectively. The values may roughly correspond to the energy gap and increase with Ca-doping.

To probe the reasons of the metal–insulator transition, we analyzed the crystal and electronic of the iridum pyrochlores. First, as observed above, neither intensity nor wave number of the peaks vary with temperature in x=0.2 and 0.4 samples. The low-temperature x-ray diffraction experiment [17] on polycrystalline samples of A=Nd, Eu and Pr also showed that all three compounds keep cubic pyrochlore structure down to 4 K. Therefore, it is affirmed that the main origin of the MIT here is not due to the crystal-structure phase transition from the pyrochlore structure. From Raman spectra for different doping samples at 300 k, we found that the Ir–O bands elongate and the A–O′ bands turn shorter. The resistivity in $Bi_{2-x}Ca_xIr_2O_{7-\delta}$ may be increased by smaller A-site ionic radium, which increases the trigonal compression of octahedra and decreases the Ir–O orbital overlap [23,24].

Then we take the electronic structure into consideration. Ca^{2+} ions replace Bi^{3+} ions at random and it has a weaker bond. These two terms will affect the conductivity through the relaxation time τ in the following way [25]:

$$1/\tau=1/\tau\_\mathrm{d}+1/\tau\_\mathrm{ph} \quad (3)$$

In this equation τ is the relaxation time which is proportional to the electrical conductivity and depends on the 'imperfections' of the crystal, τ_d is due to the disorder introduced by Ca that occupies the same crystalline position of Bi but in a random way, τ_{ph} is the phononic term due to the oscillations of the atoms. With the introduction of Ca^{2+}, the scattering becomes more frequent, the oscillation becomes larger because of the weaker bond. As a result, the value of τ_d and τ_{ph} decrease. Hence, τ is reduced with Bi replacement by Ca and the electrical resistivity is increased [26].

These two phenomena described above induced by Ca doping cause the decreasing in the conductivity. Meanwhile, we noticed that the substitution of Ca^{2+}, with a smaller ionic radius changes the local geometry around Ir [5,7,24]. Thus, it is necessary to further study the frustrated magnetic properties

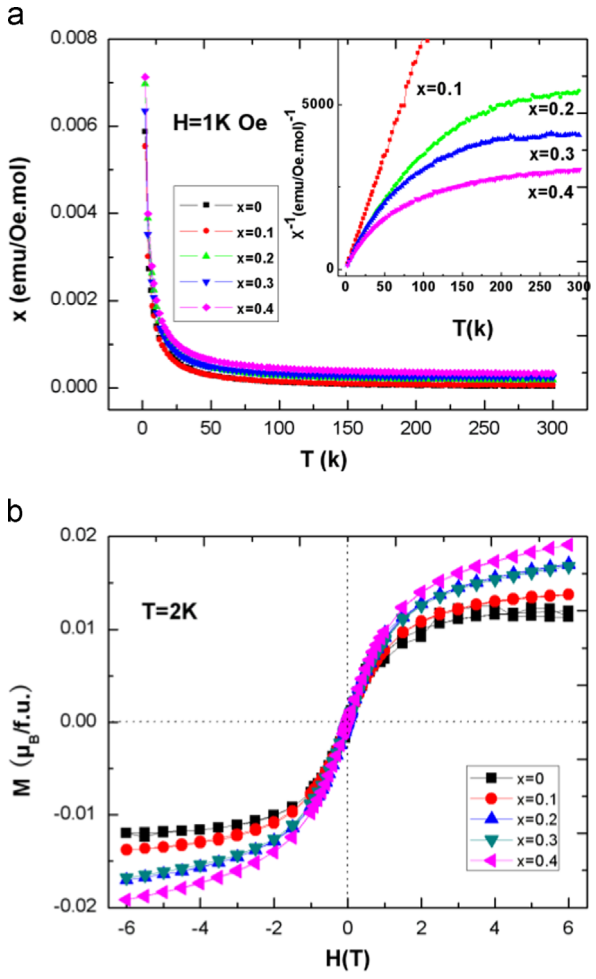

Fig. 4. (a) The magnetic susceptibility χ as a function of temperature and χ^{-1} fitting curves under magnetic field $H=1$ kOe; (b) Isothermal magnetization M versus H at $T=2$ K.

of this series. The magnetic susceptibilities of $Bi_{2-x}Ca_xIr_2O_{7-\delta}$ ($0 \le x \le 0.4$) samples were taken through zero field cooling (ZFC) and field cooling (FC) method. We did not observe essential difference of χ(T) between ZFC and FC conditions until 2 K for all the samples. Fig. 4(a) shows the DC magnetic susceptibilities plotted as a function of temperature under 1 kOe for them. The isothermal magnetization $M(H)$ (seen in Fig. 4(b)) were measured from -6 T to 6 T at 2 K. The saturation magnetization increases with Ca content increases.

As can be observed from Fig. 4(a), none of the samples shows a magnetic transition at least down to 2 K, and the magnetic susceptibility increases with the Ca doping. We fitted $\chi(T)$ for the high temperature range to Curie–Weiss (CW) law,

$$\chi\_((T)) = \chi\_0 + \alpha T + C/(T-\theta) \quad (4)$$

The CW temperature θ and Curie constant C are tabulated in Table 1. For the low doping ($x=0$–0.2) samples, the CW temperature θ are negative, with Ca doping, the constant increases, and turn into positive. The C values decrease and increase, accordingly. The change of θ and C indicates the weakening of the AFM interaction. In addition, from the isothermal magnetization curves $M(H)$ (seen in Fig.4(b)), we observed that the magnetic moments do not reach saturation until the magnetic field increase to 6 T, for the high levels of $x=0.2$, 0.3 and 0.4. The positive θ values and the increasing magnetization indicate that there may be a possible enhancing FM.

As observed in the recent studies [27,28], the substitution of A^{3+} by lower valence cation will increase the valence state of Ir from 4+ to 5+. In the pyrochlore iridates, $A_2Ir_2O_7$, the Ir^{4+} has an unpaired $J_{eff}=1/2$ electron, but the Ir^{5+} has an empty $J_{eff}=1/2$ level, and hence has no net moment. As a result, the replacement of Ir^{4+} by Ir^{5+} may favor a decreasing anti-ferromagnetism. And the mixed valence states of Ir may lead to a double-exchange interaction: the O2p electron hops to the empty $J_{eff}=1/2$ orbital of Ir^{5+}, and then the $J_{eff}=1/2$ electron on the nearby Ir^{4+} hops to the O2p orbital. This double-exchange interaction between Ir^{5+} and Ir^{4+} through the oxygen 2p orbital may give rise to ferromagnetism.

Fig. 5 shows the Specific heat $C(T)$, entropy $S(T)$ and magnetic portion of $C(T)$, $C_m(T)$ as a function of temperature for $x=0$, 0.2 and 0.4 samples. As shown in Fig. 5(a), we did not observe the second-order phase transition from $C(T)$ at the corresponding temperature of MIT. Meanwhile, the illustrated linear behavior of $C(T)/T$ for parent sample as a function of T^2 at low temperature (inset in Fig.5(a)) indicates that $C(T)$ can be well described by [18]

$$C\_((T)) = \gamma T + \beta T \circ 3 \quad (5)$$

where γ measures the effective mass or the DOS near E_F, and β measures the phonon and/or magnetic contributions. However for the Ca-doped samples ($x=0.2$ and 0.4), the formula is not available, which probably because of the disorder and large oscillation introduced by Ca doping. [21] The entropy $S(T)$, derived from the integration of $C(T)/T$, reduces with Ca doping, shown in Fig. 5(b). Considering the effects of Ca^{2+}

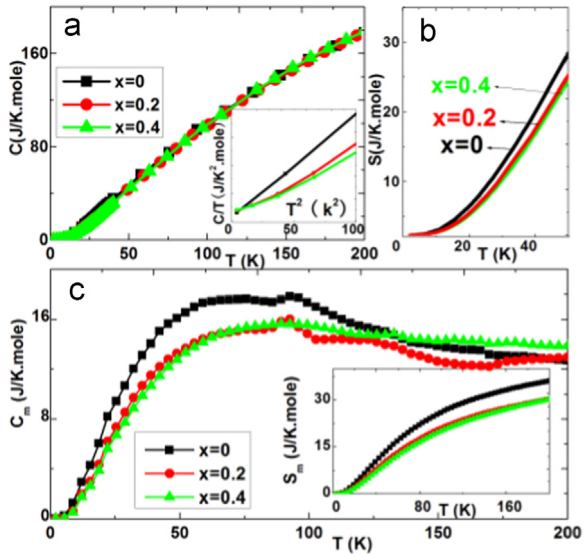

Fig. 5. (a) (b) and (c) Specific heat $C(T)$, entropy $S(T)$ and magnetic portion of $C(T)/C_m(T)$ as a function of temperature for $x=0$, 0.2 and 0.4 samples, respectively; the inset in figure (a) and (c) shows $C(T)/T$ as a function of T^2 below 10 K and the magnetic entropy $S_m(T)$ estimated from C_m/T, as described in the text.

on the Bi^{3+} site, we could infer that the decrease of entropy is induced by the enhancement of magnetic order.

Fig. 5(c) shows the magnetic specific heat $C_m(T)$ and the magnetic entropy $S_m(T)$ for $x=0$, 0.2 and 0.4 samples. In order to obtain the magnetic specific heat $C_m(T)$ of the samples, we subtracted the lattice contribution by using the specific heat of nonmagnetic $Bi_2Ti_2O_7$ measured under the same condition, and then integrated $C_m(T)/T$ to obtain the magnetic entropy $S_m(T)$ of the systems. The $C_m(T)$ is suppressed by increasing of x, the values of the magnetic entropy $S_m(T)$ are reduced. The doping of Ca^{2+} reduces the angle of Ir–O–Ir and lengthens the Ir–O bands, as a result the spin in limit becomes larger and the magnetic order is enhanced.

4. Conclusion

In this work, we performed systematic study of the crystal structure, electrical transport and magnetic properties of the prototypically pyrochlore iridate $Bi_{2-x}Ca_xIr_2O_{7-\delta}$. Due to the lengthening of Ir–O bands and the enhancing of disorder and phononic oscillations inducing by Ca^{2+} doping, the electrical conductivity was reduced and the metal–insulator transition was observed. Magnetic measurements on the system indicate a shift of Ir towards +5 in the doping samples. Magnetic transition was not observed, but the positive value of θ for high doping sample indicates a possible AF under the AFM background. Discontinuities and thermal hysteresis of magnetism were not observed at approximate T_{MIT}, indicating that the MIT might be a second-order transition.

Acknowledgments

This work was supported by the Nature Science Foundation of China (Grant nos. 11174290, U1232142 and U1332140), and Anhui Provincial Natural Science Foundation (Grant no. 1308085MA11).

References

[1] Xiangang Wan, A.M. Turner, A. Vishwanath, S.Y. Savrasov, Topological semimetal and Fermi-arc surface states in the electronic structure of pyrochlore iridates, Phys. Rev. B 83 (2011) 205101.
[2] W. Witczak-Krempa, Y.B. Kim, Topological and magnetic phases of interacting electrons in the pyrochlore iridates, Phys. Rev. B 85 (2012) 045124.
[3] H. Sagayama, D. Uematsu, T. Arima, K. Sugimoto, Determination of long-range all-in-all-out ordering of Ir^{4+} moments in a pyrochlore iridate $Eu_2Ir_2O_7$ by resonant x-ray diffraction, Phys. Rev. B 87 (2013) 100403(R).
[4] S.M. Disseler, S.R. Giblin, C. Dhital, K.C. Lukas, S.D. Wilson, M. J. Graf, Magnetization and Hall effect studies on the pyrochlore iridate $Nd_2Ir_2O_7$, Phys. Rev. B 87 (2013) 060403.
[5] Xiangang Wan, Ari Turner, Ashvin Vishwanath, Sergey Y. Savrasov, Electronic structure of pyrochlore iridates: from topological dirac metal to mott insulator, arXiv 1007 (2010) 0016.
[6] M. Kargarian, J. Wen, G.A. Fiete, Competing exotic topological insulator phases in transition-metal oxides on the pyrochlore lattice with distortion, Phys. Rev. B 83 (2011) 165112.
[7] M. Kargarian, G.A. Fiete, Topological crystalline insulators in transition metal oxides, Phys. Rev. Lett. 110 (2013) 156403.
[8] L. Savary, L. Balents, Coulombic quantum liquids in spin-1/2 pyrochlores, Phys. Rev. Lett. 108 (2012) 037202.
[9] Kyo-Hoon Ahn, Kwan-Woo Lee, Warren E. Pickett, Spin-orbit interaction driven collective electron-hole excitations in a noncentrosymmetric nodal loop Weyl semimetal, Phys. Rev. B 92 (2015) 115149.
[10] T.L. Hughes, E. Prodan, B.A. Bernevig, Inversion-symmetric topological insulators, Phys. Rev. B 83 (2011) 245132.
[11] A.M. Turner, Y. Zhang, R.S.K. Mong, A. Vishwanath, Quantized response and topology of magnetic insulators with inversion symmetry, Phys. Rev. B 85 (2012) 165120.
[12] Xiangang Wan, Jinming Dong, Sergey Y. Savrasov, Calculated magnetic and electronic properties of pyrochlore iridates, arXiv 1003 (2010) 3414.
[13] K. Ueda, J. Fujioka, Y. Takahashi, T. Suzuki, S. Ishiwata, Y. Taguchi, Y. Tokura, Variation of charge dynamics in the course of metal–insulator transition for pyrochlore-type $Nd_2Ir_2O_7$, Phys. Rev. Lett. 109 (2012) 136402.
[14] Jun J. Ishikawa, Eoin C.T. O'Farrel, Saturo Nakatsuji, Continuous transition between ferromagnetic insulator and paramagnetic metal in the pyrochlore iridate $Eu_2Ir_2O_7$, Phys. Rev. B 85 (2012) 245109.
[15] P.J. Baker, J.S. Moller, F.L. Pratt, W. Hayes, S.J. Blundell, T. Lancaster, T.F. Qi, G. Cao, Weak magnetic transitions in pyrochlore $Bi_2Ir_2O_7$, Phys. Rev. B 87 (2013) 180409(R).
[16] Sudhir K. Pandey, Kalobaran Maiti, Importance of Coulomb correlation and spin-orbit coupling in a 5d pyrochlore: $Pr_2Ir_2O_7$, Phys. Rev. B 82 (2010) 035110.
[17] Hiroshi Takatsu, Kunihiko Watanabe, Kazuki Goto, Hiroaki Kadowaki, Comparative study of low-temperature x-ray diffraction experiments on $R_2Ir_2O_7$ (R=Nd, Eu, and Pr), Phys. Rev. B 90 (2014) 235110.
[18] T.F. Qi, O.B. Korneta, Xian gang Wan, L.E. DeLong, P. Schlottmann, G. Cao, Strong magnetic instability in correlated metallic $Bi_2Ir_2O_7$, J. Phys.: Condens. Matter 24 (2012) 345601.
[19] M.L. Sanjuán, C. Guglieri, S. Díaz-Moreno, G. Aquilanti, A.F. Fuentes, L. Olivi, J. Chaboy, Raman and x-ray absorption spectroscopy study of the phase evolution induced by mechanical milling and thermal treatments in $R_2Ti_2O_7$ pyrochlores, Phys. Rev. B 84 (2011) 104207.
[20] T. Hasegawa, N. Ogita, K. Matsuhira, S. Takagi, M. Wakeshima, Y. Hinatsu, M. Udagawa, Raman scattering study in iridium pyrochlore oxides, J. Phys.: Conf. Ser. 200 (2010) 012054.
[21] S. Brown, H.C. Gupta, J.A. Alonso, M.J. Martinez-Lope, Lattice dynamical study of optical modes in $Tl_2Mn_2O_7$ and $In_2Mn_2O_7$ pyrochlores, Phys. Rev. B 69 (2004) 054434.
[22] D.J. Arenas, L.V. Gasparov, J.C. Wei Qiu, Charles H. Nino, Patterson, D. B. Tanner, Raman study of phonon modes in bismuth pyrochlores, Phys. Rev. B 82 (2010) 214302.
[23] H.J. Koo, M.H. Whangbo, B.J. Kennedy, Similarities and differences in the structural and electronic properties of ruthenium and iridium pyrochlores $A_2M_2O_{7-y}$ (M=Ru, Ir), J. Solid State Chem. 136 (1998) 269–273.
[24] William Witczak-Krempa, Gang Chen, Yong Baek Kim, Leon Balents, Correlated quantum phenomena in the strong spin-orbit regime, Annu. Rev. Conds. Matter Phys. 5 (2014) 57–58.
[25] N.W. Ashcroft, N.D. Mermin, Solid State Physics, Holt-Saunders International Editions, London, 1976 (Chapters 13 and 16).
[26] C. Cosio-Castaneda, P. de la Mora, G. Tavizon, Synthesis and structural analysis of $Bi_{2-y}Sr_yIr_2O_7$ a new pyrochlore solid solution, J. Solid State Chem. 184 (2011) 1251.
[27] P. de la Mora, C. Cosio-Castaneda, F. Morales, R. Escudero, G. Tavizon, Magnetic behavior of the the $Bi_{2-y}Sr_yIr_2O_7$ pyrochlore solid solution, J. Solid State Chem. 200 (2013) 49–53.
[28] w K. Zhu, M. Wang, B. Seradjeh, Fengyuan Yang, S.X. Zhang, Enhanced weak ferromagnetism and conductivity in hole-doped pyrochlore iridate $Y_2Ir_2O_7$, Phys. Rev. B 90 (2014) 054419.